Drifting Maneuver Investigation via Phase Plane Analysis of Experimental Data

Giovanni Righetti, Guido Napolitano dell'Annunziata, Flavio Farroni, Matteo Massaro, and Basilio Lenzo(✉)

Department of Industrial Engineering, University of Padova, Padua, Italy
basilio.lenzo@unipd.it

Abstract. This paper presents a comprehensive analysis of experimental data on drifting maneuvers, using vehicle data collected by Stanford University with a professional driver. Vehicle dynamics during drifting, characterised by high sideslip angles and countersteering, are examined. By using a nonlinear single track model with nonlinear tires, this study compares real-car data to simulated models within a phase-plane framework. It also explores the application of saddle-node bifurcation theory to understand the abrupt changes in vehicle behaviour during drifting.

Keywords: vehicle dynamics · drifting · phase-plane · experiments

1 Introduction

The study and analysis of drifting maneuvers gives relevant information about vehicle attitude when negotiating a turn in the nonlinear range of tyre characteristics. Drifting is commonly referred to as an unstable cornering condition, associated to large vehicle sideslip angles and countersteering [1]. Maintaining the control of the car in such situations is very challenging, so that only professional drivers are able to cope and even manage this vehicle behaviour. Among others, the saddle-node bifurcation theory - often applied in nonlinear dynamics and mathematics - is a useful tool to examine the sudden and abrupt changes in vehicle behavior during drifting maneuvers [2].

Several papers deal with vehicle drifting and focus on control strategies to stabilise it [3]. Voser et al. [4] propose a steering controller for autonomously performing high sideslip manoeuvres through a nonlinear single track model-based controller. Stanford University's vehicle dynamics group combines drifting control, path tracking and brake-based speed control [5]. Edelmann et al. [6] develop a driver model able to compute the necessary driver inputs to keep the vehicle in a large sideslip manoeuvre.

This work aims at giving a thorough and exhaustive analysis of experimental data concerning drifting manoeuvres, performed by professional driver Ken Gushi and collected by Stanford University, using the electric DeLorean prototype MARTY [7]. Real-car data are compared to a simple nonlinear single track model, by visualising vehicle states in a phase plane framework. Moreover, the relationship between drift and saddle-node bifurcation phenomenon is discussed.

G. Mastinu et al. (Eds.): AVEC 2024, LNME, pp. 22–28, 2024.
https://doi.org/10.1007/978-3-031-70392-8_4

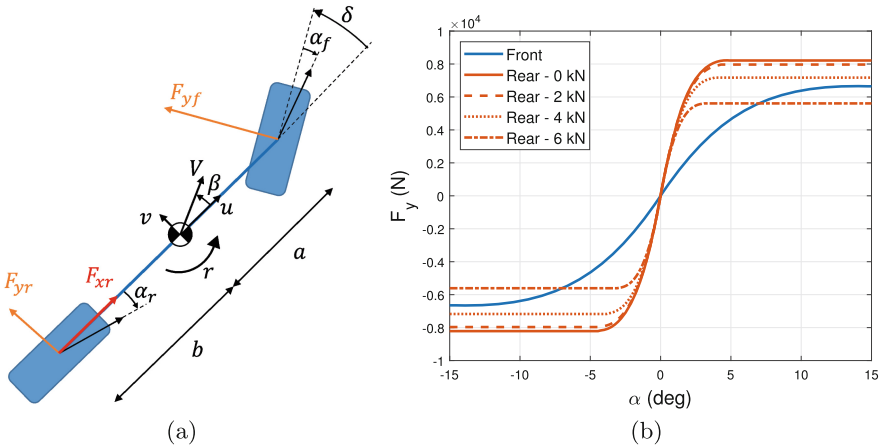

Fig. 1. (a) Schematic of the single track model. β is the vehicle sideslip angle. (b) Axle characteristics, with the rear one depicted for different values of F_{xr}.

Table 1. Main vehicle and tire parameters.

Parameter	Symbol	Value	Parameter	Symbol	Value
Mass	m	1700 kg	Front cornering stiff.	$C_{\alpha f}$	75 kN/rad
Yaw moment of inertia	I_{zz}	2385 kg m^2	Rear cornering stiff.	$C_{\alpha r}$	275 kN/rad
COG to front axle dist.	a	1.392 m	Front friction coeff.	μ_f	0.95
COG to rear axle dist.	b	1.008 m	Rear friction coeff.	μ_r	0.85

2 Vehicle and Tire Model

Figure 1a shows the used 3-degree-of-freedom (dof) single track model. The vehicle state includes longitudinal velocity, u, lateral velocity, v, yaw rate, r:

$$\dot{u} = \frac{1}{m}\Big[-F_{yf}\sin(\delta) + F_{xr}\Big] + vr \tag{1}$$

$$\dot{v} = \frac{1}{m}\Big[F_{xf}\sin(\delta) + F_{yf}\cos(\delta) + F_{yr}\Big] - ur \tag{2}$$

$$\dot{r} = \frac{1}{I_{zz}}\Big[a\big(F_{xf}\sin(\delta) + F_{yf}\cos(\delta)\big) - bF_{yr}\Big] \tag{3}$$

where F_{yf} and F_{yr} are the front and rear lateral forces, F_{xr} is the rear longitudinal force, δ is the steering angle at wheel. Since the experimental vehicle MARTY is rear wheel drive and the driver does not brake, the front longitudinal force $F_{xf} = 0$. Symbols and values of other relevant parameters are in Table 1.

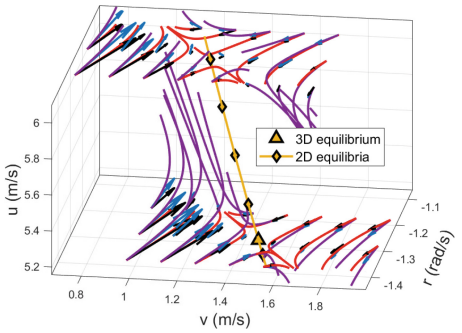

Fig. 2. v-r-u phase portrait. Purple and red curves are trajectories of the 3-dof and 2-dof systems, respectively. Blue and black arrows are vectors tangent to the trajectories of the 3-dof and 2-dof systems. Yellow diamonds are unstable equilibria for the 2-dof system, for various u. The yellow triangle is an unstable equilibrium of the 3-dof system.

Lateral forces are modelled using the slip Fiala tire model. For a generic tire:

$$\begin{cases} F_y = \ C_\alpha \tan\alpha - \dfrac{C_\alpha^2}{3F_{y,\max}}|\tan\alpha|\tan\alpha + \dfrac{C_\alpha^3}{27F_{y,\max}^2}\tan^3\alpha, & |\alpha| \leq \alpha_s \\ F_y = F_{y,\max}\text{sgn}(\alpha), & \text{otherwise} \end{cases} \tag{4}$$

where C_α is the axle cornering stiffness and $F_{y,\max}$ is the maximum available axle lateral force, calculated using the friction circle theory:

$$F_{y,\max} = \sqrt{(\mu F_z)^2 - F_x^2} \tag{5}$$

where F_z is the vertical load and μ the friction coefficient. Kinematic equations define front and rear tire slip angles $\alpha_f = \delta - \arctan\left(\frac{v+ar}{u}\right)$, $\alpha_r = -\arctan\left(\frac{v-br}{u}\right)$, while α_s is the maximum slip angle beyond which the tire starts to slide: $\alpha_s = \arctan\left(\frac{3F_{y,max}}{C_\alpha}\right)$. The axle characteristics are shown in Figure 1b.

3 Phase Plane and Space Representation

The dynamics of the vehicle model may be effectively represented via three-dimensional u-v-r phase portrait. The derivatives of the state variables are computed point-wise from equations of motion (1) (2) and (3). Hence, for each point (u_0, v_0, r_0) a vector $\mathbf{t}$ composed by the three state derivatives is associated, $\mathbf{t} = \dot{v}\,\hat{\mathbf{v}} + \dot{r}\,\hat{\mathbf{r}} + \dot{u}\,\hat{\mathbf{u}}$, where $\hat{\mathbf{v}}$, $\hat{\mathbf{r}}$ and $\hat{\mathbf{u}}$ are the unit vectors of the three axes of the graph. $\mathbf{t}$ defines the direction of vehicle state's time evolution. The same may be done for the 2-dof case, obtaining a 2-dimensional vector $\mathbf{t}_2$ defined by $\dot{v}$ and $\dot{r}$ for a given u. Since in both 2 and 3-dof systems $\dot{v}$ and $\dot{r}$ are computed by solving equations (2) and (3), the projections of 3D vectors $\mathbf{t}$ on a $v - r$ plane coincide with the directions of 2D vectors $\mathbf{t}_2$. This is in line with the results in [8]. In this work equilibrium *curves* may be distinguished in a $v - r - u$ phase

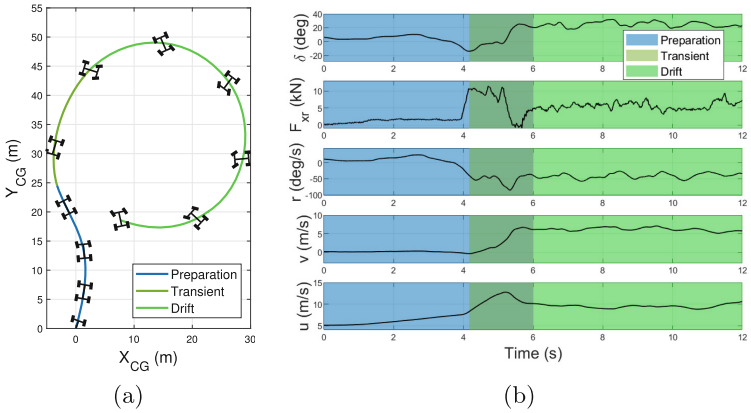

Fig. 3. (a) Trajectory and wheel orientation; (b) Time history.

space, Fig. 2, which are composed by the equilibrium *points* of $v-r$ phase planes computed at every vehicle speed (for fixed driver inputs). One relevant consequence is that equilibria of the 3-dof system are located on equilibrium curves, since they are constrained by the same lateral and yawing motion equations. Moreover, even if 2D equilibria cannot be classified as equilibria of the 3-dof system as well, $\dot{v}$ and $\dot{r}$ are zero in correspondence of equilibrium curves, and 2D and 3D trajectories behave similarly in their neighborhood.

On this basis, both 3D and 2D portraits are exploited for analysing experimental data and relate actual vehicle states to the studied vehicle model.

4 Experimental Data and Drift Phases

For space constraints, a single representative maneuver is analyzed. Figure 3 shows the vehicle path and the orientation of the wheels, along with relevant data. Graphs are split in 3 phases: *preparation*, *transient* and *drift*. As soon as the driver countersteers (end of the *preparation* phase) vehicle states evolve (*transient*) to reach the condition of a (quasi) steady-state manoeuvre (*drift*), with large β, steering angle oscillating around 25 deg and longitudinal force around 5.6 kN. It is interesting to note that: i) while the steering angle sign changes, the sign of the yaw rate does not; ii) both lateral velocity and yaw rate are kept almost constant by the driver, justifying the hypothesis of (quasi) steady-state; iii) the longitudinal velocity is also almost constant, even though, as discussed in previous section, that is not strictly required to drift.

5 Drift Equilibrium Analysis

Figure 4a presents the actual vehicle state in a 3D phase space fashion. It is compared to saddle equilibria of the 2D system, computed for steering angle

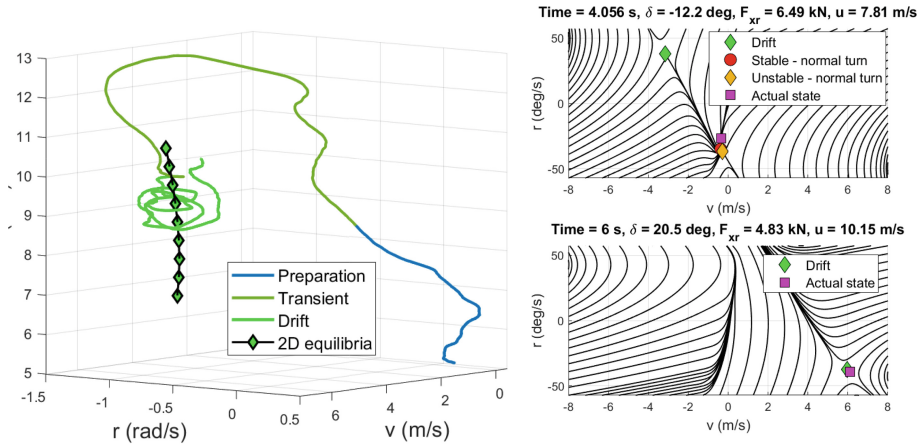

(a) (b)

Fig. 4. (a) 3D portrait of the actual vehicle state evolution; (b) v-r phase plane (top) just before saddle-node bifurcation and (bottom) at the beginning of controlled drift.

and rear traction force equal to their mean values in the drift phase. It can be appreciated that the driver actively controls the vehicle stability and, in doing so, he keeps the vehicle in the neighborhood of the black curve. Figure 4b compares the phase plane of the system just before bifurcation [1] (4.056 s, three equilibria) and at the beginning of the controlled drift (6.000 s, only one equilibrium). The actual state of the vehicle is close to the stable-normal turn equilibrium [1] in the preparation phase, while it gradually moves toward drift after bifurcation.

Figure 5 shows that the time instant of bifurcation and the one the driver countersteers are very close, endorsing the goodness of the nonlinear single track model. When the steering rate changes sign (beginning of the transient), the driver has quickly brought rear traction to the limit, and he then maintains it for a while. This is probably done by the driver to maximise the yaw moment resulting on the vehicle, favouring the entrance in a drifting condition (with pretty much all the grip used longitudinally, equation (5) is ≈ 0). The procedure followed by the driver in the transient is then dictated by the need to stabilise the vehicle and it has a similar pattern to the one described in [9].

Another relevant insight is that yaw rate of the controlled drift is comparable to the one at the beginning of transient. Since it is a quasi-steady-state condition, the manoeuvre can be classified as an almost constant radius one. An important application of this would be autonomous drifting, where a vehicle is asked to carry out a turn of predetermined cornering radius , or the implementation of drift as a strategy to minimise lap-time (e.g. in Rally).

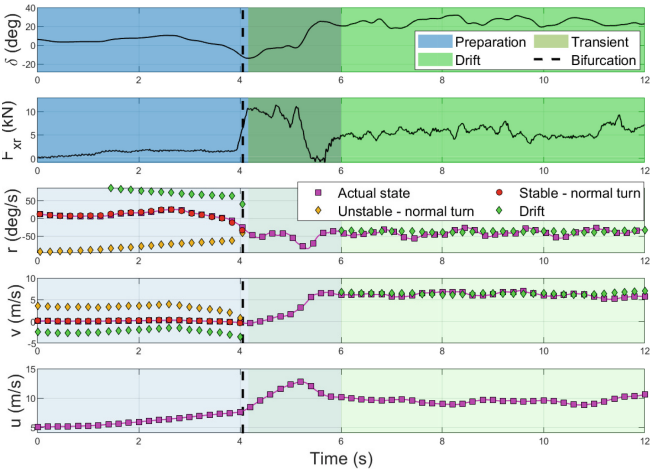

Fig. 5. Analysis of the drifting procedure. v and r are compared to 2D equilibria at each time instant with the nomenclature in [1], note the trends before/after bifurcation.

6 Conclusion

The paper provided a comprehensive understanding of the dynamics involved in vehicle drifting manoeuvres, emphasizing the critical role of saddle-node bifurcation theory in interpreting these complex scenarios. The proposed analysis, grounded in both experimental data and simple yet insightful models, highlights the intricate interplay between vehicle control, tire dynamics, and driver inputs during drifting. This could lead to innovations in vehicle safety and performance.

References

1. Righetti, G., Binetti, E., de Castro, R.P., Lot, R., Massaro, M., Lenzo, B.: On the investigation of car steady-state cornering equilibria and drifting. Technical report, SAE Technical Paper (2024)
2. Rossa, F.D., Mastinu, G., Piccardi, C.: Bifurcation analysis of an automobile model negotiating a curve. Veh. Syst. Dyn. **50**(10), 1539–1562 (2012)
3. Velenis, E., Frazzoli, E., Tsiotras, P.: On steady-state cornering equilibria for wheeled vehicles with drift. In: Proceedings of the 48h IEEE Conference on Decision and Control (CDC) held jointly with 2009 28th Chinese Control Conference, pp. 3545–3550. IEEE (2009)
4. Voser, C., Hindiyeh, R.Y., Gerdes, J.C.: Analysis and control of high sideslip manoeuvres. Veh. Syst. Dyn. **48**(S1), 317–336 (2010)
5. Goel, T.: In Complete Control Simultaneous Path Speed and Sideslip Angle Control of a Drifting Automobile. PhD thesis, Stanford University (2022)
6. Edelmann, J., Plöchl, M., Pfeffer, P.: Analysis of steady-state vehicle handling and driver behaviour at extreme driving conditions. na (2011)

7. Goh, J.Y., Gerdes, J.C.: Simultaneous stabilization and tracking of basic automobile drifting trajectories. In: 2016 IEEE Intelligent Vehicles Symposium (IV), pp. 597–602. IEEE (2016)
8. Beal, C.E., Boyd, C.: Coupled lateral-longitudinal vehicle dynamics and control design with three-dimensional state portraits. Veh. Syst. Dyn. **57**(2), 286–313 (2019)
9. Vignati, M., Sabbioni, E., Cheli, F.: A torque vectoring control for enhancing vehicle performance in drifting. Electronics **7**(12), 394 (2018)